



Article

Synthesis, and Anticancer Evaluation of 4-[(Indol-3-yl)-arylmethyl]-1-phenyl-3-methyl-5-pyrazolone Derivatives via a Magnetic Aminated Starch Biocatalyst

Ali Ramshini¹, Shefa Mirani Nezhad¹, Seied Ali Pourmousavi^{1,*}, Ehsan Nazarzadeh Zare^{1,*}, Mona Pourjafar² and Esmaeel Sharifi^{3,4}

¹ School of Chemistry, Damghan University, Damghan 3671645667, Iran; ramshinali8@gmail.com (A.R.); shefamirani@yahoo.com (S.M.N.)

² Research Center for Molecular Medicine, Hamadan University of Medical Sciences, Hamadan 6517838636, Iran; pourjafar_mona@yahoo.com

³ Cancer Research Center, Hamadan University of Medical Sciences, Hamadan 6517838636, Iran; esmaeel.sharifi@gmail.com

⁴ Department of Tissue Engineering and Biomaterials, School of Advanced Medical Sciences and Technologies, Hamadan University of Medical Sciences, Hamadan 6517838636, Iran

* Correspondence: pourmousavi@du.ac.ir (S.A.P.); ehsan.nazarzadehzare@gmail.com or e.nazarzadeh@du.ac.ir (E.N.Z.)

Abstract: An eco-friendly biocatalyst was constructed in three steps. In the first step, the tosylated starch (TsST) was synthesized by using a 4-toluenesulfonyl chloride. In the second step, the aminated starch was synthesized via the reaction of TsST with para-phenylenediamine. In the third step, the magnetic biocatalyst was fabricated by an in situ coprecipitation process from ferric and ferrous salts in the existence of aminated starch (AST). The biocatalyst was characterized by ¹H NMR, EDX, FESEM, FTIR, VSM, and TGA analyses. The magnetic aminated starch (MAST) was used as a biocatalyst for the synthesis of 4-[(indol-3-yl)-arylmethyl]-1-phenyl-3-methyl-5-pyrazolone derivatives. The various products were prepared in noteworthy yields (85–93%) in fast reaction times (35–80 min) without laborious work-up procedures. The anticancer evaluation of some 4-[(indol-3-yl)-arylmethyl]-1-phenyl-3-methyl-5-pyrazolones derivatives was studied on the survival rate of breast cancer cell lines (MCF-7) and human fibroblast cells by using an MTT assay. Additionally, recovery of the biocatalyst was studied, and results showed that the MAST was easily isolated from the reaction flask and could be recycled for up to six consecutive cycles without meaningfully falling in its efficiency.

Keywords: biocatalysis; magnetic aminated starch; pyrazolone derivatives; anticancer



Citation: Ramshini, A.; Nezhad, S.M.; Pourmousavi, S.A.; Nazarzadeh Zare, E.; Pourjafar, M.; Sharifi, E. Synthesis, and Anticancer Evaluation of 4-[(Indol-3-yl)-arylmethyl]-1-phenyl-3-methyl-5-pyrazolone Derivatives via a Magnetic Aminated Starch Biocatalyst. *Catalysts* **2023**, *13*, 908. <https://doi.org/10.3390/catal13050908>

Academic Editor: Jean-Marc Campagne

Received: 5 May 2023
Revised: 17 May 2023
Accepted: 19 May 2023
Published: 20 May 2023



Copyright: © 2023 by the authors. Licensee MDPI, Basel, Switzerland. This article is an open access article distributed under the terms and conditions of the Creative Commons Attribution (CC BY) license (<https://creativecommons.org/licenses/by/4.0/>).

1. Introduction

In the last decade, the use of heterogeneous catalysts in organic reactions has been greatly extended because they have great value in terms of the environment and economy. The use of heterogeneous catalysts is preferable to homogeneous catalysts because the establishment of the active species on the heterogeneous substrate increases the stability of the catalyst, reduces waste, simplifies the test procedures, slows reaction conditions, and is known for having easy extraction and recycling of the catalyst. Among the different materials, inorganic nanoparticles and functionalized polymers are the most popular supports for heterogeneous catalytic applications [1,2].

Nowadays, most sciences and technologies focus on eco-friendly and sustainable sources and procedures. In this respect, the use of biopolymers, which are inexpensive and easily available, biodegradable, biocompatible, and nontoxic, is very attractive for any useful purpose. From the catalytic point of view, these polymers have several remarkable features, such as high functionality and biodegradability, which make them attractive for utilization as support [3,4].

Among the biopolymers, starch has been extensively studied, owing to its availability, low cost, and usability in the food industry. Starch has extremely weak mechanical strength and can be combined with a variety of nanofillers to enhance its stability. In addition, the water resistance of starch can be enhanced by including nanoparticles [5]. In this regard, natural polymer-based nanocomposites have been established due to their excellent physicochemical properties as suitable options for catalyst applications [6].

On the other hand, combining magnetic nanoparticles with biopolymers has opened many opportunities for the development of organic–inorganic compounds with good catalytic properties. In recent years, the use of magnetic nanoparticles as catalysts has attracted the attention of researchers due to their easy synthesis and recovery and good catalytic properties [7–9].

The pyrazolone compounds have attracted wide attention due to their variety of biological activity as antioxidant [10], antimicrobial [11,12], antiviral [13], antitumor [14], antitubercular [15], analgesic [16], hypoglycemic [17], and anti-inflammatory [18] activities. On the other hand, antipyrine is one of the first synthetic organic compounds to be used as an important drug with a pyrazolone core. Until now, various drugs containing a pyrazolone core have been approved by the Food and Drug Administration (FDA) [19]. Synthesis of pyrazolones using different techniques and catalysts has been reported, for example, in the presence of microwave irradiation and solvent-free conditions [20], organocatalytic [21], *N, N*-dimethylformamide dimethyl acetal (DMFDMA) [22], sodium acetate [12], chiral Gd(OTf)₃/*N, N'*-dioxide complex [23], ionic liquid [24], Brønsted acid catalysts [25], and ionic liquid under ultrasonic irradiation [26].

The above methods have special advantages, but they also have disadvantages, such as time-consuming work, catalysts containing transition metals, use of hazardous bases, non-recyclable catalysts, longer reaction times, and difficult waste disposal. With these considerations in mind, developing a simple, feasible, and environmentally friendly synthesis process for pyrazolones is of significant interest.

Therefore, this study focused on the preparation of a magnetic nanocomposites based on aminated starch as a biocatalyst for the syntheses of 4-[(indol-3-yl)-arylmethyl]-1-phenyl-3-methyl-5-pyrazolones.

2. Results and Discussions

2.1. Characterization of Biocatalyst

FTIR: In the FTIR spectrum of TsST, the stretching vibrations of the -OH groups are observed at 3415 cm⁻¹ (Figure 1A). The absorption band at 2944 cm⁻¹ is related to stretching vibrations of C-H in the glucose ring, and the absorption bands at 1148, 1077, and 942 cm⁻¹ are ascribed to C-O-C, C-OH, and C-H of the glucose ring, respectively. The emergence of the absorption band at 1602 cm⁻¹ confirms the presence of C=C of the aromatic ring. The absorption bands at 1362 and 1117 cm⁻¹ can be attributed to the antisymmetric and symmetric stretching vibrations of SO₂, respectively [27]. Reducing the intensity of the SO₂ absorption bands and the emergence of the band at 3200 cm⁻¹ confirms the presence of primary and secondary amine in the spectrum of the AST. In the FTIR spectrum of MAST (Figure 1A), a broad band at 556 cm⁻¹ is related to the Fe–O–Fe stretching modes in Fe₃O₄. In addition, other distinct bands related to AST are observed in the FTIR spectrum of the MAST.

VSM: Magnetic behavior of Fe₃O₄ nanoparticles and MAST nanocomposite were investigated via VSM at room temperature. The magnetic behavior of Fe₃O₄ nanoparticles before and after being composited with MAST has been compared. The magnetization saturation values of Fe₃O₄ and MAST were 59.94 and 28.73 emu/g, respectively. The decrease in magnetic saturation in the MAST biocatalyst is proportional to the covering of magnetic Fe₃O₄ by AST, which confirmed the preparation of MAST (Figure 1B).

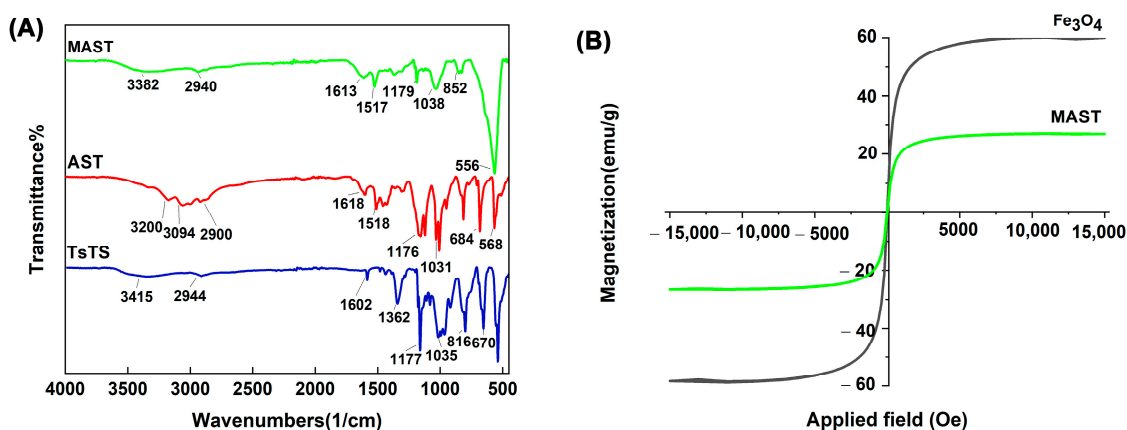


Figure 1. FTIR spectra of the TsST, AST, and MAST (A) and VSM curves of MAST and Fe₃O₄ (B).

EDX: The chemical composition of TsST, AST, and MAST was determined using EDX. Comparing the elements' peaks in the TsST with the AST shows the appearance of a new peak related to amine in the AST (Figure 2). On the other hand, the presence of an iron peak in the MAST composite compared to the AST indicates the successful preparation of the composite. The presence of small amounts of sulfur in all samples indicates the trapping of unreacted tosylate between the polymer chains (Figure 2).

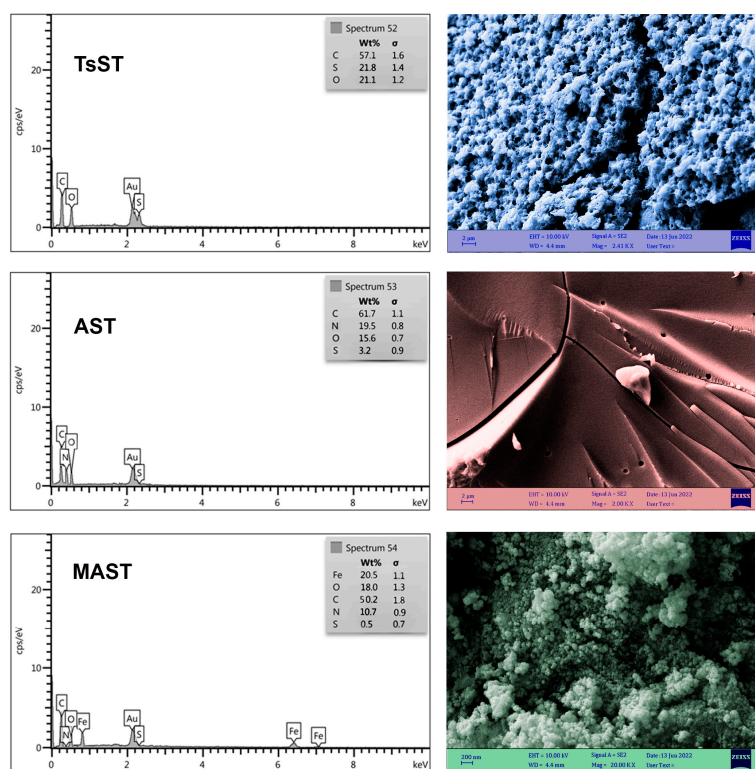


Figure 2. FESEM micrographs and EDX spectra of TsST, AST, and MAST.

FESEM: The surface morphology of prepared compounds was examined by scanning microscopy. A rough surface can be seen in the FESEM image of the TsST, while a relatively smooth surface with a series of aggregates can be seen in the image of the AST, which could be due to the amination reaction. In the FESEM image of MAST, a structure with a large accumulation of iron oxide nanoparticles is observed (Figure 2).

TG/DTG: Two weight losses are observed in TG thermograms of TsST, AST, and MAST. Evaporation of moisture and solvents adsorbed on the surface of samples caused

a weight loss below 200 °C. The weight loss in the range of 400–415 °C could be related to the removal of tosylate and amine groups in the TsST and AST, respectively. The high thermal stability with a char yield of 59.62% at 800 °C is observed in the TG thermogram of MAST compared to TsST and AST (Figure 3).

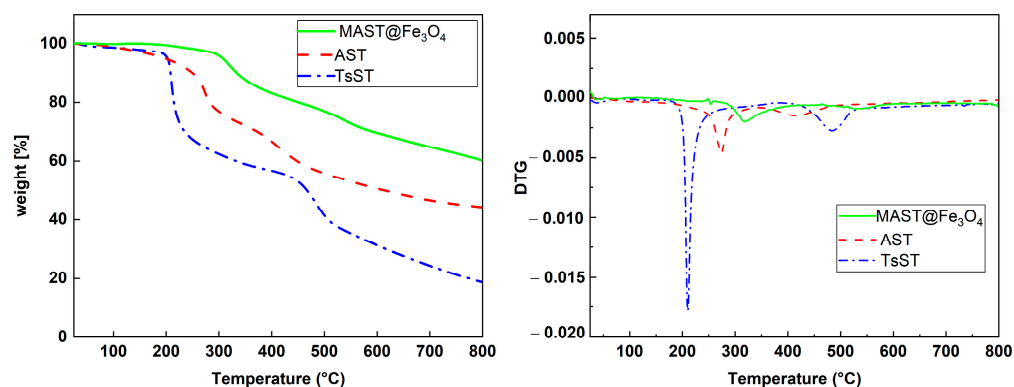


Figure 3. TG and DTG thermograms of the TsST, AST, and MAST.

^1H NMR: In the ^1H NMR spectrum of TsST, the signal at 1.23 ppm attributed to the protons of CH_3 (toluene sulfonyl), and the signals at 2.2 to 4.03 ppm, corresponded to the protons of starch backbone. The signals at 7.1–7.79 ppm are related to the C–H aromatic (toluene sulfonyl). In the ^1H NMR spectrum of AST, the signals at 7.1–7.2 ppm are related to the C–H aromatic (*p*PDA), and the signals at 7.46–7.48 ppm corresponded to the protons of primary and secondary amines (Figure 4).

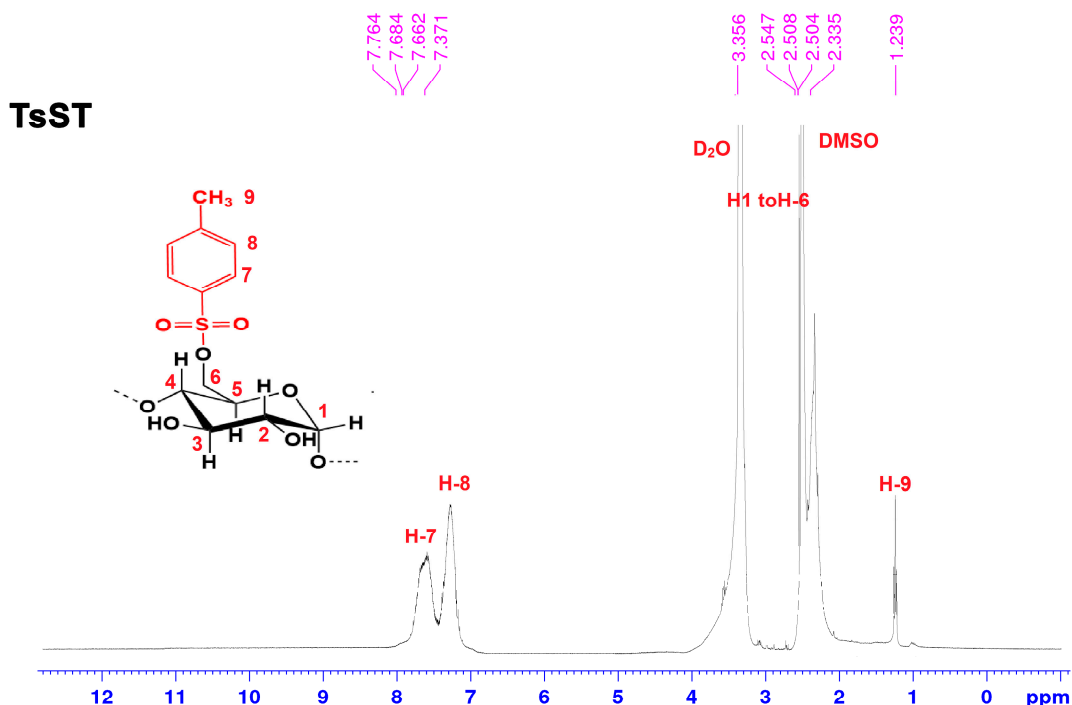


Figure 4. Cont.

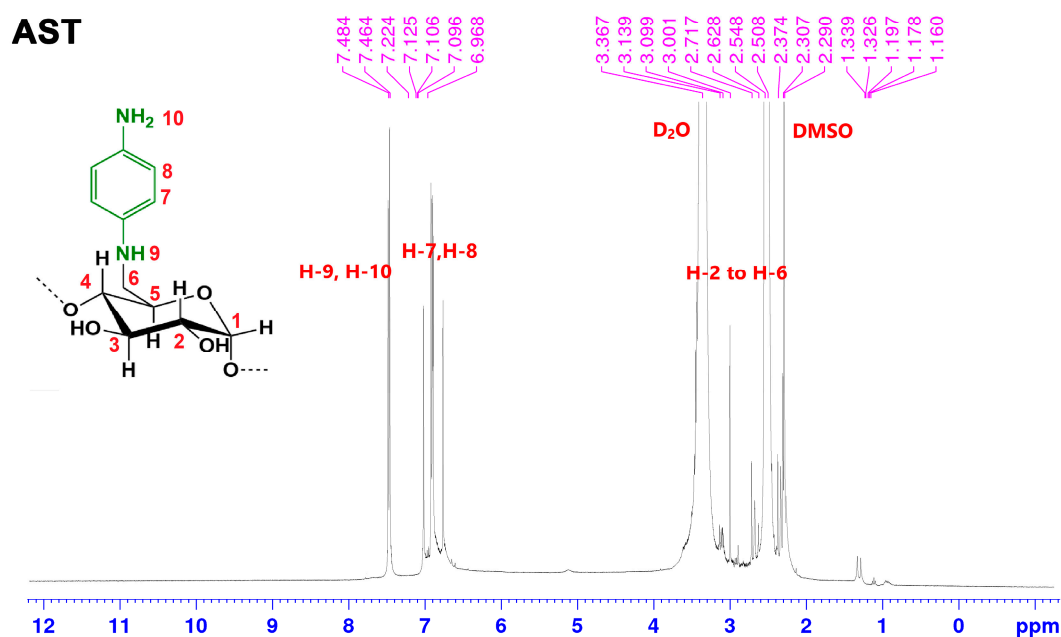


Figure 4. ¹H NMR spectra of TsST and AST in DMSO-d₆.

2.2. Investigation of the Catalytic Activity of the MAST

The MAST biocomposite with several active sites was used as an eco-friendly biocatalyst to promote the synthesis of organic compounds. In this respect, after the fabrication and characterization of the MAST biocatalyst, its catalytic activity in the synthesis of pyrazolone derivatives was evaluated. The synthesis of 4-[(indol-3-yl)-arylmethyl]-1-phenyl-3-methyl-5-pyrazolones by a condensation reaction of 3-methyl-1-phenyl-1*H*-pyrazol-5-ol, indole, and aromatic aldehyde was studied to determine the catalytic activity of the MAST biocomposite. To evaluate the reaction optimization, the reaction between indole, benzaldehyde, and 3-methyl-1-phenyl-1*H*-pyrazol-5-ol under different conditions was utilized.

In this regard, the reaction was examined in CHCl₃, THF, EtOH, water, hexane, and MeOH and under solvent-free conditions. As shown in Table 1, entries 1-7, EtOH was more suitable than other solvents and showed the highest yield for model reaction. In addition, different temperatures (e.g., 25, 40, 60, and 80 °C) were applied in the model reaction for investigating the temperature effect. The obtained results of the solvent and temperature studies showed that polar solvents, such as water, EtOH, and MeOH, decrease the reaction efficiency once the temperature increases more than 40 °C. A model reaction was also evaluated in the presence and absence of different amounts of MAST biocatalyst to study of catalytic effect of MAST in the reaction. The results showed that the reaction needs a catalyst to continue, and, in the absence of the catalyst, the efficiency is not high. In addition, the use of 0.06 g of MAST in EtOH at 40 °C for 80 min was the best condition to achieve the highest yield (87%) of the synthesized products.

To ensure that the study is not limited to the use of indole, benzaldehyde, and 3-methyl-1-phenyl-1*H*-pyrazol-5-ol only, a series of derivatives were synthesized under optimal conditions. The derivatives of 4-[(indol-3-yl)-arylmethyl]-1-phenyl-3-methyl-5-pyrazolones were synthesized in high (85%) to excellent (93%) yields by a condensation reaction of aldehyde, 3-methyl-1-phenyl-1*H*-pyrazol-5-ol, and indole in the presence of 0.06 g of the MAST nanocomposite at 40 °C (Table 2). The formation of pyrazolone derivatives was confirmed through melting points and spectral analysis, such as FTIR, ¹H-NMR, and ¹³C-NMR (Figures S1–S27).

Table 1. Optimization of the three-component reaction of 3-methyl-1-phenyl-1*H*-pyrazol-5-ol, benzaldehyde, and indole ^a.

Entry	Solvent	Catalyst (g)	Temp. (°C)	Time (Min.)	Yield (%) ^b
1	EtOH/H ₂ O	0.04	40	120	55
2	H ₂ O	0.04	40	180	30
3	THF	0.04	40	180	30
4	EtOH	0.04	40	90	75
5	MeOH	0.04	40	90	70
5	CHCl ₃	0.04	40	180	30
6	Hexane	0.04	40	180	10
7	Solvent-free	0.04	40	180	30
8	EtOH	0.04	r.t	100	60
9	EtOH	0.04	60	100	55
10	EtOH	0.04	80	100	30
11	EtOH	0.06	40	80	87
12	EtOH	0.08	40	80	88
13	EtOH	-	40	120	45

^a Reaction conditions: benzaldehyde (1 mmol), 3-methyl-1-phenyl-1*H*-pyrazol-5-ol (1 mmol), and indole (1 mmol);
^b isolated yield.

Table 2. Synthesis of 4-[(indol-3-yl)-arylmethyl]-1-phenyl-3-methyl-5-pyrazolones by MAST and benzaldehyde derivatives ^a.

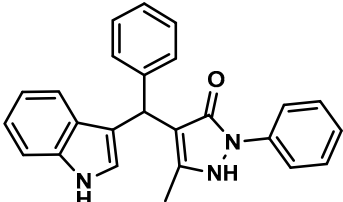
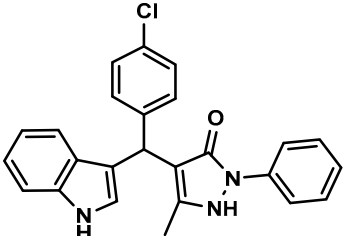
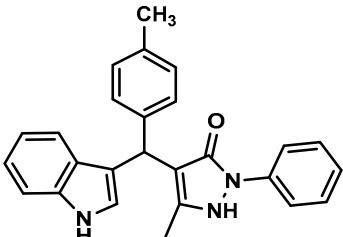
Entry	Product	Code	Time (min.)	Yield (%) ^b	M.P. (°C)		Ref.
					Observed	Reported	
1		6a	80	87	233–234	235–236	[28]
2		6b	60	90	178–179	173–175	[28]
3		6c	70	87	182–183	180–182	[28]

Table 2. Cont.

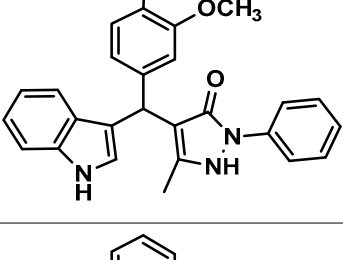
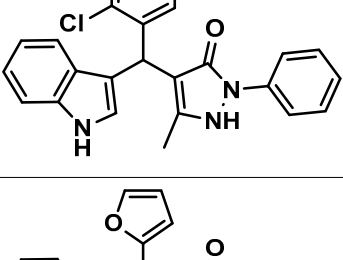
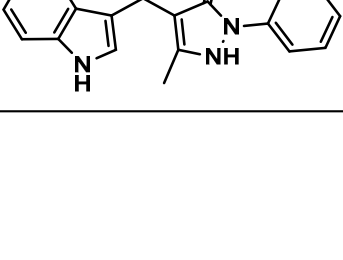
Entry	Product	Code	Time (min.)	Yield (%) ^b	M.P. (°C)		Ref.
					Observed	Reported	
4		6d	65	88	170–173	170–171	[28]
5		6e	35	93	184–186	184–186	[28]
6		6f	40	90	239–241	242–244	[28]
7		6g	65	89	195–197	206	[29]
8		6h	70	89	162–164	161–163	[28]
9		6i	60	91	194–195	191–193	[28]

Table 2. Cont.

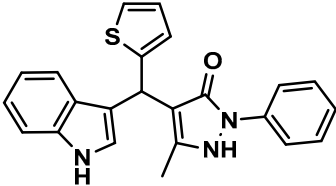
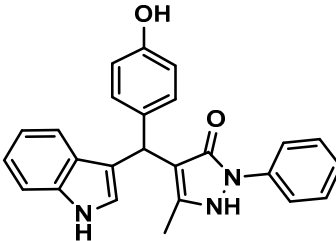
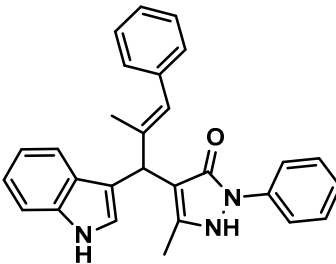
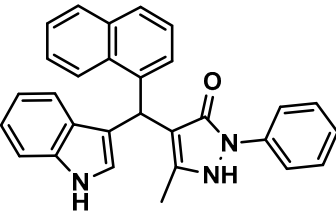
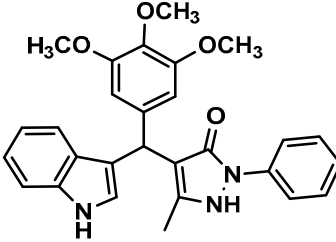
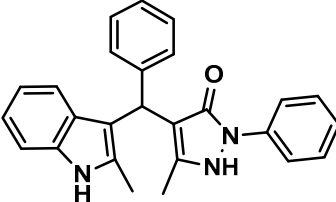
Entry	Product	Code	Time (min.)	Yield (%) ^b	M.P. (°C)		Ref.
					Observed	Reported	
10		6j	50	90	241–243	242–244	[30]
11		6k	90	85	245–246	246	[29]
12		6l	80	86	149–151	NR	
13		6m	70	90	213–215	NR	
14		6n	90	88	187–190	NR	
15		6o	70	87	211–213	210–212	[30]

Table 2. Cont.

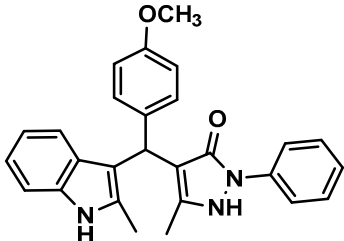
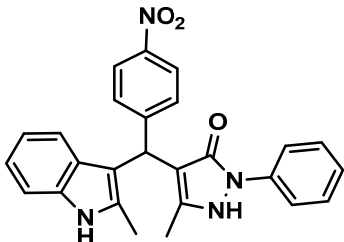
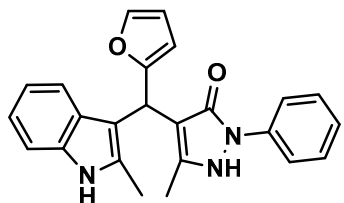
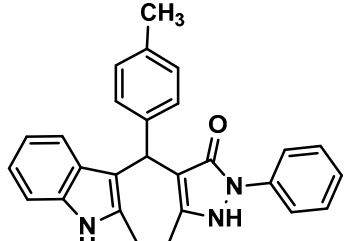
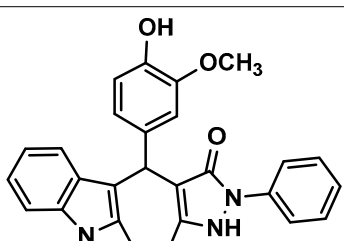
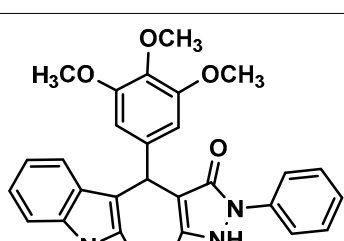
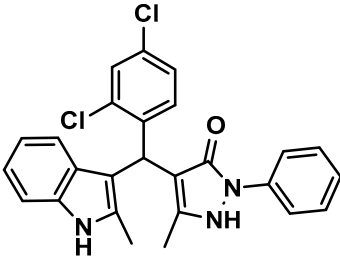
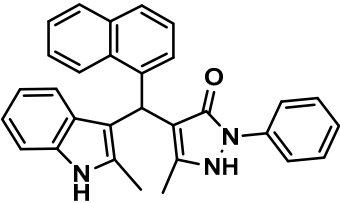
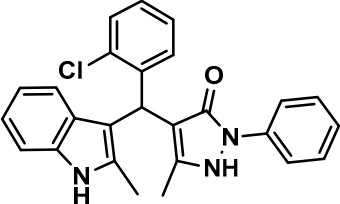
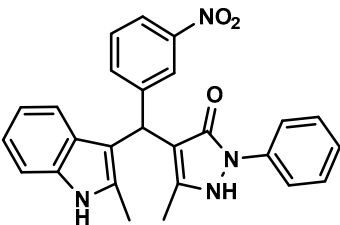
Entry	Product	Code	Time (min.)	Yield (%) ^b	M.P. (°C)		Ref.
					Observed	Reported	
16		6p	50	85	195–196	193–195	[30]
17		6q	30	90	232–234	231–233	[30]
18		6r	40	91	187–188	185–187	[30]
19		6s	50	85	188–189	185–187	[30]
20		6t	65	86	182–185	NR	
21		6u	90	89	194–197	NR	

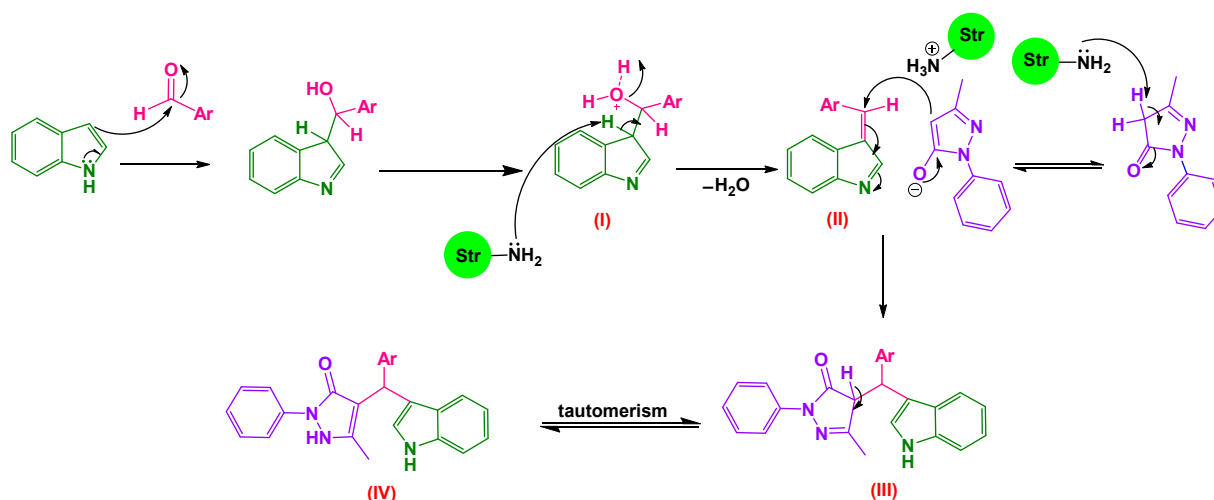
Table 2. Cont.

Entry	Product	Code	Time (min.)	Yield (%) ^b	M.P. (°C)		Ref.
					Observed	Reported	
22		6v	35	92	180–182	NR	
23		6w	70	89	200–203	NR	
24		6x	60	90	161–163	NR	
25		6y	50	92	225–228	NR	

^a Reaction conditions: indole (1 mmol), aromatic aldehyde (1 mmol), 3-methyl-1-phenyl-1*H*-pyrazol-5-ol (1 mmol), (5 mL) EtOH, and MAST (0.06 g) at 40 °C; ^b isolated yield. NR: not reported.

2.2.1. Proposed Mechanism

The proposed mechanism of the catalytic reaction in the presence of the MAST is shown in Scheme 1. In this mechanism, indole first attacks the carbonyl group of the aldehyde, and, after the water removal, intermediate (II) is formed. Next, 3-methyl-1-phenyl-1*H*-pyrazol-5-ol deprotonation by the biocatalyst is carried out. The reaction is then followed by the Michael's addition of 3-methyl-1-phenyl-1*H*-pyrazol-5-ol to convert intermediate (II) to (III). In the end, intermediate (III) was converted into product (IV) by tautomerization.



Scheme 1. The proposed mechanism for the synthesis of 4-[(indol-3-yl)-arylmethyl]-1-phenyl-3-methyl-5-pyrazolones catalyzed by MAST.

2.2.2. Recovery

Reusability and recyclability are important features of heterogeneous catalytic systems in green chemistry. The reusability and recycling of the MAST biocatalyst for the pyrazolones synthesis were studied. We examined the recovery study in the synthesis of the **6a** derivative in the optimized conditions. After completing the reaction, the MAST biocatalyst was isolated by a magnet from the reaction mixture. It was employed for six consecutive runs/turns after its washing with H₂O/EtOH (Figure 5). It was observed that the recovered MAST biocatalyst can be employed in the reaction without a noteworthy reduction in product yield.

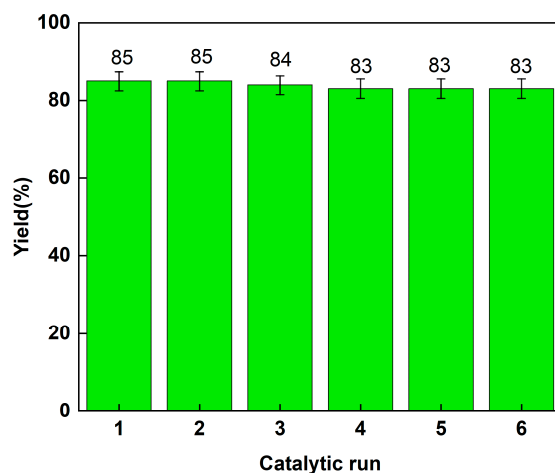


Figure 5. MAST reusability in the synthesis 4-((1H-indol-3-yl)(phenyl)methyl)-3-methyl-1-phenyl-1H-pyrazole-5-ol (**6a**).

2.3. In-Vitro Anticancer Study

The effect of the 4-[(indol-3-yl)-arylmethyl]-1-phenyl-3-methyl-5-pyrazolones derivatives on the survival rate of breast cancer (MCF-7) and normal cells was investigated using an MTT assay. The MCF-7 and human fibroblast cells were treated with various concentrations of 4-[(indol-3-yl)-arylmethyl]-1-phenyl-3-methyl-5-pyrazolones derivatives (150, 75, 37.5, 18.75, 9.375 $\mu\text{g}/\text{mL}$) for 24 and 48 h. As shown in Figure 6, treatment of MCF-7 with these derivatives reduced the percentage of viable cells compared with untreated cells in a dose and time-dependent manner ($p < 0.001$). Moreover, the cell viability in human

fibroblast cells was significantly higher when treated with the derivatives compared to MCF-7. Hence, these derivatives can be lethal to cancerous cells while protecting normal cells from cytotoxic effects.

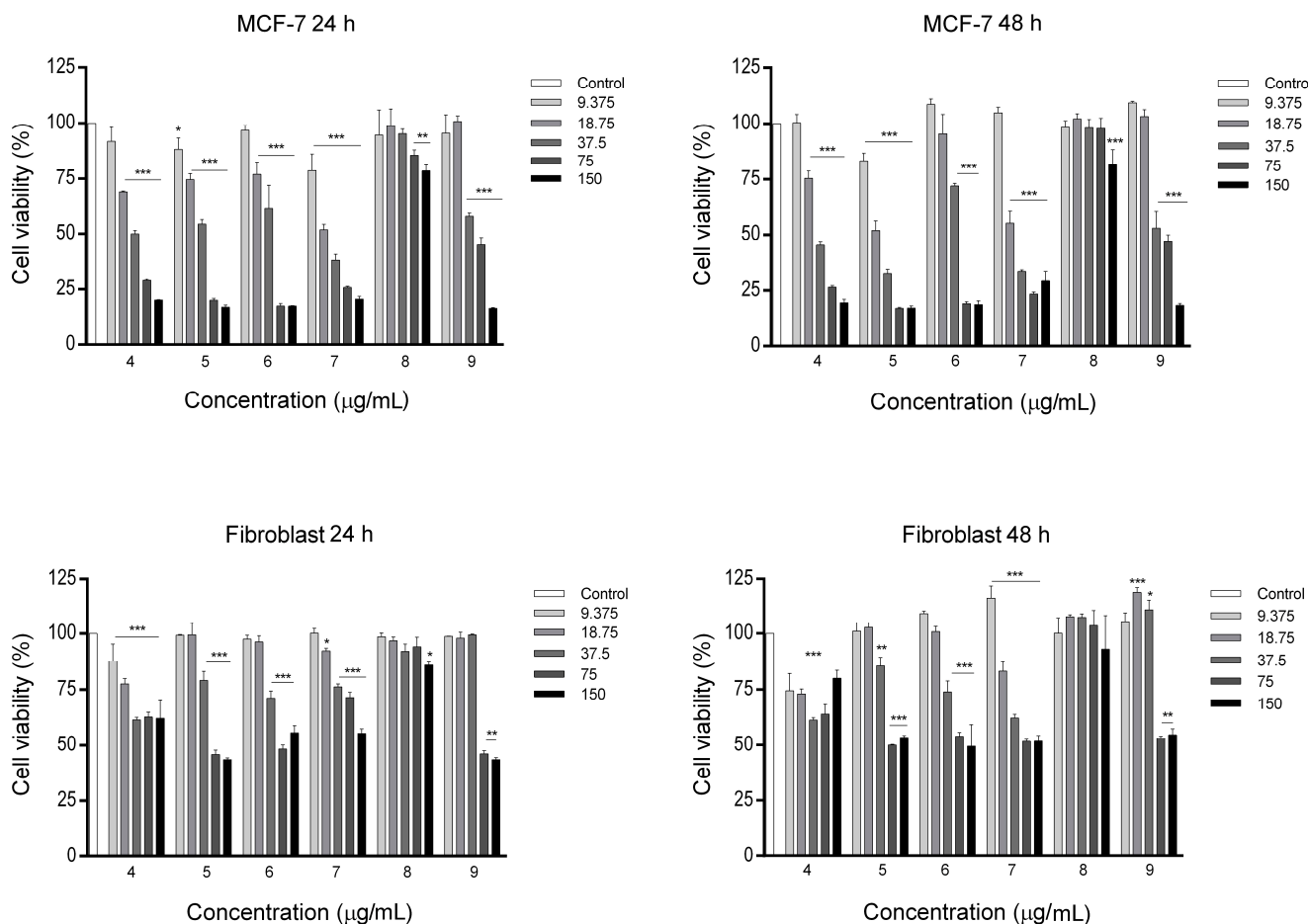


Figure 6. Cellular toxicity assessment of 4-[(indol-3-yl)-arylmethyl]-1-phenyl-3-methyl-5-pyrazolones derivatives using MTT assay in MCF-7 and human fibroblast cells after 24 and 48 h of incubation. Data are represented as mean \pm standard error of the mean ($n = 3$). * $p < 0.05$, ** $p < 0.01$ and *** $p < 0.001$ compared with control group.

As is seen in Table 3, the 50% inhibition concentrations (IC₅₀) values of **6n** for MCF-7 cells were 25.8 and 21.8 $\mu\text{g}/\text{mL}$ after 24 and 48 h respectively, and less than other derivatives (**6j**, **6l**, **6p**, **6r**, and **6y**). Our results showed that the high concentrations (35, 75, and 150 $\mu\text{g}/\text{mL}$) of the 4-[(indol-3-yl)-arylmethyl]-1-phenyl-3-methyl-5-pyrazolone derivatives lead to ~50% lethality of MCF-7 cancer cells. The IC₅₀ for doxorubicin in different breast cancer cell lines, including MCF-7, reported being in a range between 0.68 and 5.074 $\mu\text{g}/\text{mL}$ [31,32]. In a study performed by Lovitt et al. [33], IC₅₀ for doxorubicin-resistant MCF-7 and MDA-MB-231 breast cancer cell lines was 225.2 ± 64.2 nM and 87.7 ± 10.6 nM, respectively. However, these conventional anticancer medications often exhibit significant toxicity toward healthy cells due to their lack of specificity. Treatment with 100 μM and 0.1 μM of doxorubicin results in 83.64% and 25.14% fibroblast cell viability, respectively. These findings highlight the deleterious impact of doxorubicin on normal cells, thereby limiting its clinical utility as an antitumor agent in the treatment of cancers [34]. In contrast, 4-[(indol-3-yl)-arylmethyl]-1-phenyl-3-methyl-5-pyrazolone derivatives, when administered at high concentrations (150 $\mu\text{g}/\text{mL}$) within a 24–48 h timeframe, demonstrate significantly reduced toxicity towards normal cells (~50% lethality after treatment with 150 $\mu\text{g}/\text{mL}$ concentration for 48 h). These findings propose that 4-[(indol-3-yl)-arylmethyl]-

1-phenyl-3-methyl-5-pyrazolones derivatives may have the potential to overcome drug resistance, target specific molecular pathways, and enhance safety and tolerability in cancer treatment, compared to conventional chemotherapies, such as doxorubicin and 5FU with fewer side effects.

Table 3. In vitro cytotoxicity effect (IC50) of 4-[(indol-3-yl)-arylmethyl]-1-phenyl-3-methyl-5-pyrazolones derivatives against MCF-7 and human fibroblast cells after different exposure times.

Sample	Cell	Time (h)	
		24	48
6l	MCF-7	39.2	41.3
	Fibroblast	392.1	409.4
6p	MCF-7	38.2	23.1
	Fibroblast	70.07	150.1
6r	MCF-7	34.6	52.5
	Fibroblast	81.9	115.4
6n	MCF-7	25.8	21.3
	Fibroblast	226.8	96.6
6j	MCF-7	1660.5	11,647.4
	Fibroblast	498,041.6	597,030.5
6y	MCF-7	48.5	52.0
	Fibroblast	92.5	135.8

3. Materials and Methods

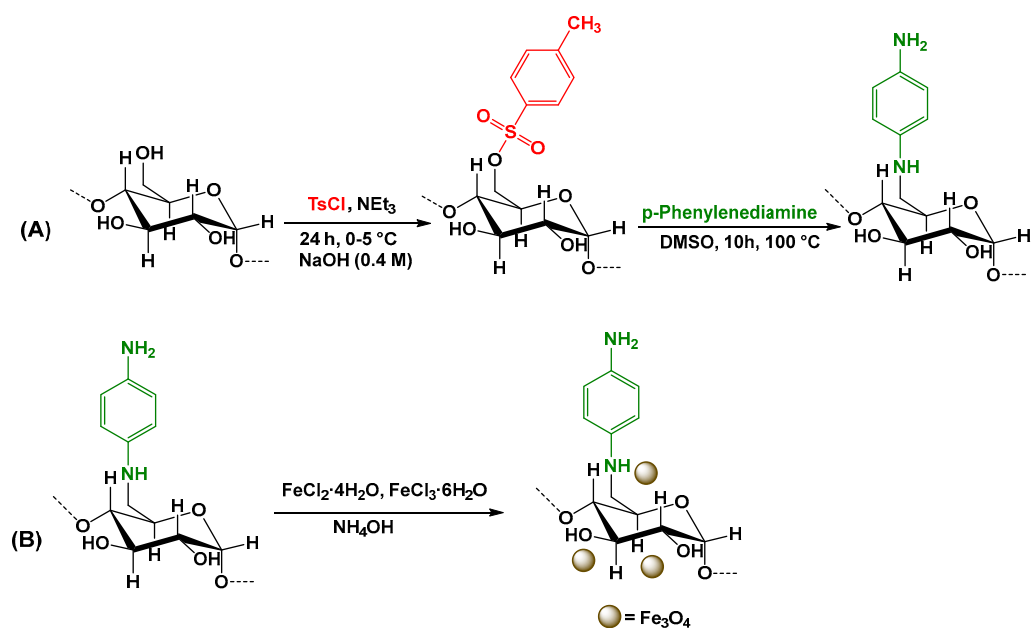
3.1. Materials and Instruments

Corn starch, 4-toluenesulfonyl chloride (TsCl), sodium hydroxide, para-phenylenediamine (*p*PDA), ferric chloride hexahydrate, ferrous chloride tetrahydrate, and all solvents were purchased from Merck Company, Darmstadt, Germany. Additionally, ethyl acetoacetate, indole, phenylhydrazine, and all other reagents were provided by Sigma-Aldrich Company, St. Louis, MO, USA.

Hydrogen and carbon nuclear magnetic resonance spectroscopy (^1H NMR and ^{13}C NMR, Bruker Avance DRX-400, Bremen, Germany), Fourier transforms infrared spectroscopy (FTIR, Bruker Tensor 27, Bremen, Germany), field emission scanning electron microscope (FESEM, Hitachi S 4160, Tokyo, Japan), vibrating-sample magnetometer (VSM, LDKFB, Meghnatis Daghigh. Kavir, Kashan, Iran) and thermogravimetric analysis (TGA, TGA 209F3, NETZSCH, Selb, Germany) were applied for the chemical characterization of the products.

3.2. Synthesis of Aminated Starch

Aminated starch (AST) was synthesized in two steps, according to the Nouri et al. [27] recipe, with minor modifications (Scheme 2A). In the first step, starch (2.0 g) was added to 50 mL of NaOH solution (0.4 M) in a 200 mL round bottom flask. After that, in an ice bath, 7 mL of triethylamine was added, drop by drop, to the dissolved starch for 30 min under stirring. TsCl solution (7 g in 20 mL of NaOH solution) was poured into the previous solution, and the final solution was then kept under stirring at 0–5 °C for 24 h. After the neutralization of the solution by HCl, the resulting precipitate was filtered and washed several times with H₂O and EtOH. Finally, tosylated starch (TsST) was dried in a vacuum oven at 50 °C for 12 h.



Scheme 2. Preparation of aminated starch (A) and magnetic aminated starch nanocomposite (B).

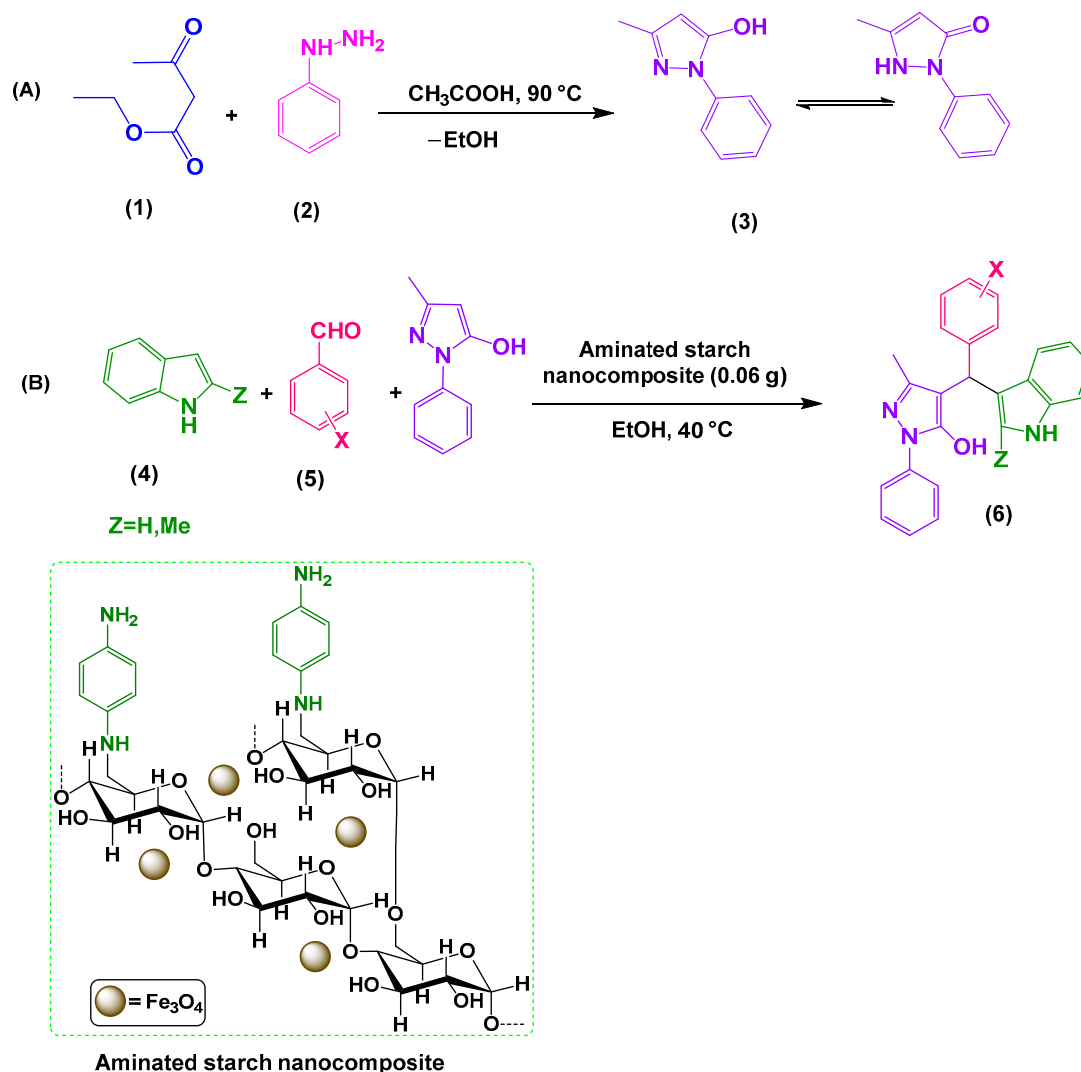
In the second step, the AST was prepared through the reaction of *p*PDA with TsST. Briefly, TsST (2.0 g) was added to 50 mL of DMSO at 80 °C. Then, *p*PDA (6.0 g) was added to the reaction mixture, and the mixture was heated to 100 °C for 10 h. In the end, the color of the reaction mixture became reddish brown. Then, the reaction mixture was cooled to room temperature, and the obtained precipitate was filtered and washed several times with H₂O and EtOH and dried at 50 °C for 12 h [27].

3.3. Preparation of Magnetic Aminated Starch

The magnetic aminated starch nanocomposite (MAST) was prepared by combining AST, ferrous chloride tetrahydrate, and ferric chloride hexahydrate salts through an in situ co-precipitation technique (Scheme 2B). Briefly, a solution of FeCl₃·6H₂O and FeCl₂·4H₂O (25 mL), with a molar ratio of 2:1, was prepared. AST (1 g) was added to the above solution at 80 °C, and then 10 mL of NH₄OH (25%) was added until the pH reached 10. The dark brown precipitate (MAST) was isolated by a magnet and washed several times with H₂O and EtOH and ultimately dried at 80 °C for 10 h.

3.4. Synthesis of 3-Methyl-1-phenyl-1H-pyrazole-5-ol: A General Procedure

3-Methyl-1-phenyl-5-pyrazolone was synthesized with an equal molar ratio of ethyl acetoacetate and phenylhydrazine in a 100 mL round bottom flask. Then, acetic acid (0.5 mL) was added to the solution, and the flask was kept under stirring for 1 h at 90 °C. After cooling the solution to room temperature, ether (25 mL) was added to the solution to obtain crystalline pyrazolone. Finally, pyrazolone crystals were filtered and purified using recrystallization in EtOH (Scheme 3A) [30].



Scheme 3. Synthesis of 3-methyl-1-phenyl-1*H*-pyrazol-5-ol (A) and of 4-[(indol-3-yl)-arylmethyl]-1-phenyl-3-methyl-5-pyrazolones (B).

3.5. Synthesis of 4-[(Indol-3-yl)-arylmethyl]-1-phenyl-3-methyl-5-pyrazolones

MAST biocatalyst (0.05 g) was added into a round bottom flask containing an equal molar ratio of indole, 3-methyl-1-phenyl-1*H*-pyrazol-5-ol, and aldehyde in EtOH (3 mL), and then the mixture was stirred at 40 °C until the reaction was completed. After the end of the reaction, the MAST biocatalyst was collected by a magnet, and the product was filtered and washed with EtOH (2 × 5 mL) (Scheme 3B).

3.6. In Vitro Cell Viability Assay

The inhibitory effects of the 4-[(indol-3-yl)-arylmethyl]-1-phenyl-3-methyl-5-pyrazolone derivatives on cell viability were evaluated using the colorimetric 3-(4,5-dimethylthiazol-2-yl)-2, 5-diphenyl tetrazolium bromide (MTT) method assay. The MCF-7 (a breast cancer cell line) and human fibroblast cells were seeded in 96-well plates at a density of 1×10^4 and 5×10^3 per well, respectively, and incubated at humidified 5% CO₂ and 37 °C overnight. Then, the cells were preserved with different concentrations of 4-[(indol-3-yl)-arylmethyl]-1-phenyl-3-methyl-5-pyrazolone derivatives (6l, 6p, 6r, 6n, 6j, and 6y) for 24 and 48 h. Thereafter, MTT solution three (5 mg/mL) was added to each well, and the plates were incubated for 1 h at 37 °C. Then, the medium was completely removed, and 100 μL of DMSO was added to each well to dissolve formazan crystals. The absorbance of solubilized

purple formazan was measured via an automatic microplate reader at 570 nm. The cells' viability percentage was considered using the following equation:

$$\text{Cell Viability \%} = \frac{\text{absorbance of treated cells}}{\text{absorbance of untreated cells}} \times 100$$

4. Conclusions

The MAST composite, as an eco-friendly biocatalyst, was prepared in three steps. The ^1H NMR and FTIR spectroscopies exhibited that the tosylation and amination of the starch were successfully performed. The VSM analysis showed that the MAST biocatalyst was superparamagnetic with a saturation magnetization of around 28.73 emu/g. The high thermal stability of the MAST biocatalyst was due to the presence of Fe_3O_4 nanoparticles in the AST matrix. The catalytic activity of MAST biocatalyst in the synthesis of 4-[(indol-3-yl)-arylmethyl]-1-phenyl-3-methyl-5-pyrazolones showed that the 0.06 g of MAST biocatalyst, to produce the desired products in a short interval of 30–90 min, is required under optimal reaction conditions. In addition, pyrazolone derivatives were obtained with a maximum yield (93%) in ethanol solvent at 40 °C for 35 min. The recovery test displayed that the MAST biocatalyst was easily separated by a magnet and showed excellent reusability at least six times without striking decreased catalytic activity. In addition, MTT assay of 4-[(indol-3-yl)-arylmethyl]-1-phenyl-3-methyl-5-pyrazolone derivatives on the survival rate of breast cancer and normal cells showed that the cell viability in human fibroblast cells was significantly high in comparison with MCF-7. These findings suggest that 4-[(indol-3-yl)-arylmethyl]-1-phenyl-3-methyl-5-pyrazolone derivatives may have the potential to overcome drug resistance, target specific molecular pathways, and enhance safety and tolerability in cancer treatment, compared to conventional chemotherapies, such as doxorubicin and 5FU with fewer side effects.

5. Spectroscopic Data

4-((4-chlorophenyl)(1H-indol-3-yl)methyl)-5-methyl-2-phenyl-1,2-dihydro-3H-pyrazole-3-one (6b, Figures S1 and S2)

m.p. 178–179 °C; FTIR (KBr) $\nu_{\text{max}}/\text{cm}^{-1}$: 3282, 3052, 1614, 1543; ^1H NMR (400 MHz, $\text{DMSO-}d_6$): δ = 1.87 (s, 3H, CH_3), 5.73 (s, 1H, benzylic), 6.91 (t, 2H, J = 7.2 Hz, aromatic), 7.06 (t, 2H, J = 7.2 Hz, aromatic), 7.16–7.23 (q, 2H, J = 8 Hz, aromatic), 7.33–7.44 (m, 6H, aromatic), 7.75–7.70 (d, 2H, J = 7.6 Hz, aromatic), 10.90 (s, 1H, NH) ppm. ^{13}C NMR (100 MHz, $\text{DMSO-}d_6$): δ = 11.94, 36.42, 112.00, 116.24, 118.59, 119.16, 121.55, 124.32, 124.74, 127.05, 128.39, 129.34, 130.65, 130.85, 136.99, 143.04.

4-((1H-indol-3-yl)(p-tolyl)methyl)-5-methyl-2-phenyl-1,2-dihydro-3H-pyrazole-3-one (6c, Figures S3 and S4)

m.p. 182–183 °C; FTIR (KBr) $\nu_{\text{max}}/\text{cm}^{-1}$: 3284, 3059, 1620, 1552, 708; ^1H NMR (400 MHz, $\text{DMSO-}d_6$): δ = 1.82 (s, 3H, CH_3), 2.27 (s, 3H, CH_3), 5.53 (s, 1H, benzylic), 6.82 (t, 1H, J = 7.2 Hz, aromatic), 6.89 (t, 1H, J = 7.6 Hz, aromatic), 7.03–7.21 (m, 7H, aromatic), 7.35–7.37 (d, 1H, J = 8 Hz, aromatic), 7.42 (t, 2H, J = 8 Hz, aromatic), 7.74–7.76 (d, 2H, J = 8 Hz, aromatic), 10.83 (s, 1H, NH) ppm. ^{13}C NMR (100 MHz, $\text{DMSO-}d_6$): δ = 21.09, 36.46, 111.88, 118.27, 118.60, 11.75, 119.26, 119.59, 121.04, 121.47, 124.19, 127.19, 128.68, 129.05, 129.18, 129.42, 130.07, 135.21, 137.01, 138.36, 140.86, 142.39.

4-((1H-indol-3-yl)(3-nitrophenyl)methyl)-5-methyl-2-phenyl-1,2-dihydro-3H-pyrazole-3-one (6e, Figures S5 and S6)

m.p. 239–241 °C; FTIR (KBr) $\nu_{\text{max}}/\text{cm}^{-1}$: 3282, 3062, 1615, 1559, 1551, 1355; ^1H NMR (400 MHz, $\text{DMSO-}d_6$): δ = 1.95 (s, 3H, CH_3), 5.67 (s, 1H, benzylic), 6.91 (t, 1H, J = 7.6 Hz, aromatic), 6.98 (br, 1H, aromatic), 7.07 (t, 1H, J = 7.6 Hz, aromatic), 7.18 (t, 1H, J = 7.2 Hz, aromatic), 7.25–7.26 (d, 1H, J = 7.2 Hz, aromatic), 7.37–7.44 (q, 3H, J = 7.6 Hz, aromatic), 7.58 (t, 1H, J = 7.6 Hz, aromatic), 7.74–7.76 (d, 2H, J = 8 Hz, aromatic), 7.79–7.81 (d, 1H, J = 6.4 Hz, aromatic), 8.07–8.09 (d, 1H, J = 8.4 Hz, aromatic), 8.16 (br, 1H, aromatic), 10.96 (s, 1H, NH) ppm. ^{13}C NMR (100 MHz, $\text{DMSO-}d_6$): δ = 12.83, 36.78, 112.26, 115.76,

119.19, 119.33, 121.53, 121.65, 123.49, 124.58, 124.97, 126.98, 129.52, 129.98, 135.75, 136.95, 146.52, 148.13.

4-(furan-2-yl(1H-indol-3-yl)methyl)-5-methyl-2-phenyl-1,2-dihydro-3H-pyrazole-3-one (6i, Figures S7 and S8)

m.p. 194–195 °C; FTIR (KBr) $\nu_{\max}/\text{cm}^{-1}$: 3273, 3065, 1607, 1549; ^1H NMR (400 MHz, DMSO- d_6): δ = 1.89 (s, 3H, CH₃), 5.55 (s, 1H, benzylic), 6.05 (s, 1H, aromatic), 6.39–4.40 (m, 1H, aromatic), 6.91–6.95 (m, 2H, aromatic), 7.06 (t, 1H, J = 7.6 Hz, aromatic), 7.20 (t, 1H, J = 7.2 Hz, aromatic), 7.31–7.38 (m, 2H, aromatic), 7.44 (t, 2H, J = 7.6 Hz, aromatic), 7.59 (br, 1H, aromatic), 7.75–7.77 (d, 2H, J = 8 Hz, aromatic), 10.91 (s, 1H, NH) ppm. ^{13}C NMR (100 MHz, DMSO- d_6): δ = 11.98, 32.10, 56.50, 109.94, 112.10, 116.93, 118.64, 118.82, 121.33, 121.68, 123.96, 124.56, 124.81, 125.50, 126.98, 127.13, 129.47, 136.87, 137.90, 184.36, 163.46.

4-(1-(1H-indol-3-yl)-2-methyl-3-phenyl allyl)-5-methyl-2-phenyl-1,2-dihydro-3H-pyrazole-3-one (6l, Figures S9 and S10)

m.p. 149–151 °C; FTIR (KBr) $\nu_{\max}/\text{cm}^{-1}$: 3268, 3091, 1615, 1554; ^1H NMR (400 MHz, DMSO- d_6): δ = 1.99 (s, 3H, CH₃), 2.04 (s, 3H, CH₃), 4.90 (s, 1H, allylic), 6.22 (s, 1H, vinylic), 6.96 (t, 1H, J = 7.6 Hz, aromatic), 7.07 (t, 1H, J = 7.6 Hz, aromatic), 7.16–7.21 (m, 4H, aromatic), 7.29–7.46 (m, 7H, aromatic), 7.79–7.81 (d, 2H, J = 8 Hz, aromatic), 10.90 (s, 1H, NH) ppm. ^{13}C NMR (100 MHz, DMSO- d_6): δ = 12.20, 21.24, 36.46, 111.95, 115.31, 118.51, 118.80, 119.42, 121.42, 124.14, 125.82, 126.45, 127.49, 128.60, 129.02, 129.35, 137.04, 138.50, 139.49.

4-((1H-indol-3-yl)(naphthalene-1-yl)methyl)-5-methyl-2-phenyl-1,2-dihydro-3H-pyrazole-3-one (6m, Figures S11 and S12)

m.p. 213–215 °C; FTIR (KBr) $\nu_{\max}/\text{cm}^{-1}$: 3281, 3094, 1612, 1556; ^1H NMR (400 MHz, DMSO- d_6): δ = 2.3 (s, 3H, CH₃), 5.53 (s, 1H, benzylic), 7.19 (t, 3H, J = 7.2 Hz, aromatic), 7.39 (t, 4H, J = 7.6 Hz, aromatic), 7.43–7.56 (m, 3H, aromatic), 7.75–7.77 (d, 5H, J = 8 Hz aromatic), 7.91–7.93 (d, 1H, J = 8 Hz, aromatic), 8.10 (br, 1H, aromatic), 14.57 (s, 1H, NH) ppm. ^{13}C NMR (100 MHz, DMSO- d_6): δ = 12.87, 31.49, 105.01, 118.66, 120.41, 124.04, 125.16, 125.59, 125.70, 126.36, 127.17, 129.20, 131.23, 134.12, 138.36, 138.78, 145.94, 157.93.

4-((1H-indol-3-yl)(3,4,5-tri methoxyphenyl)methyl)-5-methyl-2-phenyl-1,2-dihydro-3H-pyrazole-3-one (6n, Figures S13)

m.p. 187–190 °C; FTIR (KBr) $\nu_{\max}/\text{cm}^{-1}$: 3277, 3083, 1604, 1549; ^1H NMR (400 MHz, DMSO- d_6): δ = 1.98 (s, 3H, CH₃), 3.66 (s, 3H, OCH₃), 3.69 (s, 6H, OCH₃), 5.64 (s, 1H, benzylic), 6.70–6.97 (m, 4H, aromatic), 7.65 (t, 1H, J = 7.2 Hz, aromatic), 7.17–7.38 (m, 3H, aromatic), 7.43 (t, 2H, J = 7.6 Hz, aromatic), 7.77–7.79 (d, 2H, J = 7.6 Hz aromatic), 10.78 (s, 1H, NH) ppm.

5-methyl-4-((2-methyl-1H-indol-3-yl)(4-nitrophenyl)methyl)-2-phenyl-1,2-dihydro-3H-pyrazole-3-one (6q, Figures S14 and S15)

m.p. 232–234 °C; FTIR (KBr) $\nu_{\max}/\text{cm}^{-1}$: 3271, 3092, 1608, 1547, 1544, 1351; ^1H NMR (400 MHz, DMSO- d_6): δ = 2.11 (s, 6H, CH₃), 5.95 (s, 1H, benzylic), 6.72 (t, 3H, J = 8 Hz, aromatic), 6.84–6.86 (d, 2H, J = 8 Hz, aromatic), 6.92 (t, 2H, J = 7.2 Hz, aromatic), 7.19–7.33 (m, 6H, aromatic), 10.82 (s, 1H, NH) ppm. ^{13}C NMR (100 MHz, DMSO- d_6): δ = 13.04, 17.24, 37.14, 118.20, 118.33, 123.07, 123.25, 124.86, 125.10, 125.42, 128.86, 129.24, 129.34, 129.39, 129.59, 129.79, 131.48, 135.70, 135.77, 138.64, 144.50, 146.48, 149.07.

4-(furan-2-yl(2-methyl-1H-indol-3-yl)methyl)-5-methyl-2-phenyl-1,2-dihydro-3H-pyrazole-3-one (6r, Figures S16 and S17)

m.p. 187–188 °C; FTIR (KBr) $\nu_{\max}/\text{cm}^{-1}$: 3273, 3096, 1605, 1547; ^1H NMR (400 MHz, DMSO- d_6): δ = 1.82 (s, 3H, CH₃), 2.11 (s, 3H, CH₃), 5.55 (s, 1H, benzylic), 6.00 (d, 1H, J = 2.8 Hz, aromatic), 6.42 (br, 1H, aromatic), 6.81 (t, 1H, J = 7.6 Hz, aromatic), 6.91–7.23 (m, 5H, aromatic), 7.42 (t, 2H, J = 8.4 Hz, aromatic), 7.61 (br, 1H, aromatic), 7.72–7.74 (m, 2H, aromatic), 10.79 (s, 1H, NH) ppm. ^{13}C NMR (100 MHz, DMSO- d_6): δ = 12.35, 12.33, 32.38, 49.17, 110.70, 111.73, 113.27, 118.66, 118.85, 120.23, 124.85, 124.94, 125.46, 127.14, 128.03, 128.14, 129.26, 132.26, 132.85, 135.46, 146.98.

4-((4-hydroxy-3-methoxyphenyl)(2-methyl-1H-indol-3-yl)methyl)-5-methyl-2-phenyl-1,2-dihydro-3H-pyrazole-3-one (6t, Figures S18 and S19)

m.p. 182–185 °C; FTIR (KBr) $\nu_{\max}/\text{cm}^{-1}$: 3410, 3254, 3099, 1613, 1559; ^1H NMR (400 MHz, DMSO- d_6): δ = 2.31 (s, 6H, CH₃), 3.67 (s, 3H, OCH₃), 4.95 (s, 1H, benzylic), 6.68 (br, 2H, aromatic), 6.85 (br, 2H, aromatic), 7.25–7.87 (m, 8H, aromatic), 12.40 (br, 2H, OH), 14.04 (s, 1H, NH) ppm. ^{13}C NMR (100 MHz, DMSO- d_6): δ = 11.77, 19.04, 30.31, 49.08, 55.97, 56.51, 111.16, 11.90, 116.54, 118.64, 119.00, 120.22, 121.33, 124.21, 127.12, 127.66, 129.32, 129.85, 131.53, 137.01, 148.55, 157.05.

5-methyl-4-((2-methyl-1H-indol-3-yl)(3,4,5-tri methoxyphenyl)methyl)-2-phenyl-1,2-dihydro-3H-pyrazole-3-one(6u, Figures S20 and S21)

m.p. 194–197 °C; FTIR (KBr) $\nu_{\max}/\text{cm}^{-1}$: 3223, 3081, 1606, 1558, 1012; ^1H NMR (400 MHz, DMSO- d_6): δ = 2.08 (s, 6H, CH₃), 3.54 (s, 6H, OCH₃), 3.65 (s, 3H, OCH₃), 5.87 (s, 1H, benzylic), 6.56 (br, 2H, aromatic), 6.71 (t, 2H, J = 7.6 Hz, aromatic), 6.89 (t, 4H, J = 7.6 Hz, aromatic), 7.20–7.21 (d, 1H, J = 7.6 Hz aromatic), 7.90–7.92 (d, 1H, J = 7.6 Hz, aromatic), 8.23 (s, 1H, aromatic), 10.72 (s, 1H, NH) ppm. ^{13}C NMR (100 MHz, DMSO- d_6): δ = 12.45, 13.62, 56.23, 56.50, 60.62, 110.77, 112.50, 112.79, 118.39, 118.83, 119.06, 120.04, 121.25, 125.12, 125.76, 128.69, 128.97, 129.32, 129.43, 132.39, 135.46, 136.32, 138.65, 140.36, 142.71, 149.22.

4-((2,4-dichlorophenyl)(2-methyl-1H-indol-3-yl)methyl)-5-methyl-2-phenyl-1,2-dihydro-3H-pyrazole-3-one(6v, Figures S22 and S23)

m.p. 180–182 °C; FTIR (KBr) $\nu_{\max}/\text{cm}^{-1}$: 3219, 3095, 1612, 1553, 770; ^1H NMR (400 MHz, DMSO- d_6): δ = 2.28 (s, 6H, CH₃), 5.09 (s, 1H, benzylic), 7.25 (t, 2H, J = 7.2 Hz, aromatic), 7.40–7.46 (m, 5H, aromatic), 7.556–7.561 (d, 1H, J = 2 Hz, aromatic), 7.69–7.70 (m, 5H, aromatic), 13.89 (s, 1H, NH) ppm. ^{13}C NMR (100 MHz, DMSO- d_6): δ = 12.28, 19.03, 31.83, 56.50, 103.52, 107.32, 110.54, 121.10, 126.17, 127.46, 129.33, 129.41, 131.91, 132.13, 133.37, 137.56, 138.95, 146.43.

5-methyl-4-((2-methyl-1H-indol-3-yl)(naphthalene-1-yl)methyl)-2-phenyl-1,2-dihydro-3H-pyrazole-3-one(6w, Figures S24 and S25)

m.p. 200–203 °C; FTIR (KBr) $\nu_{\max}/\text{cm}^{-1}$: 3217, 3078, 1608, 1556; ^1H NMR (400 MHz, DMSO- d_6): δ = 1.95 (s, 3H, CH₃), 2.31 (s, 3H, CH₃), 5.53 (s, 1H, benzylic), 6.64 (t, 1H, J = 7.2 Hz, aromatic), 6.77–6.79 (d, 1H, J = 6.4 Hz aromatic), 6.87 (t, 1H, J = 7.6 Hz, aromatic), 7.15–7.22 (m, 3H, aromatic), 7.33–7.55 (m, 5H, aromatic), 7.73–7.97 (m, 4H, aromatic), 10.79 (s, 1H, NH) ppm. ^{13}C NMR (100 MHz, DMSO- d_6): δ = 12.87, 15.32, 31.49, 105.11, 118.75, 120.43, 124.34, 125.15, 126.56, 125.70, 125.96, 127.18, 129.32, 131.23, 134.32, 138.36, 138.78, 145.18, 157.75.

4-((2-chlorophenyl)(2-methyl-1H-indol-3-yl)methyl)-5-methyl-2-phenyl-1,2-dihydro-3H-pyrazole-3-one(6x, Figures S26 and S27)

m.p. 161–163 °C; FTIR (KBr) $\nu_{\max}/\text{cm}^{-1}$: 3224, 3081, 1614, 1554, 772; ^1H NMR (400 MHz, DMSO- d_6): δ = 2.290 (s, 6H, CH₃), 5.14 (s, 1H, benzylic), 7.21–7.32 (m, 4H, aromatic), 7.39–7.46 (m, 4H, aromatic), 7.68–7.70 (m, 4H, aromatic), 7.79–7.80 (d, 1H, J = 7.2 Hz aromatic), 13.93 (s, 1H, NH) ppm. ^{13}C NMR (100 MHz, DMSO- d_6): δ = 12.33, 19.16, 36.73, 112.06, 115.73, 119.00, 119.09, 121.56, 121.65, 123.19, 124.58, 124.97, 126.92, 129.33, 129.94, 135.75, 136.95, 146.52, 148.12.

Supplementary Materials: The following supporting information can be downloaded at: <https://www.mdpi.com/article/10.3390/catal13050908/s1>, Figure S1: ^1H -NMR spectrum of **6b**, Figure S2: ^{13}C -NMR spectrum of **6b**, Figure S3: ^1H -NMR spectrum of **6c**, Figure S4: ^{13}C -NMR spectrum of **6c**, Figure S5: ^1H -NMR spectrum of **6e**, Figure S6: ^{13}C -NMR spectrum of **6e**, Figure S7: ^1H -NMR spectrum of **6i**, Figure S8: ^{13}C -NMR spectrum of **6i**, Figure S9: ^1H -NMR spectrum of **6l**, Figure S10: ^{13}C -NMR spectrum of **6l**, Figure S11: ^1H -NMR spectrum of **6m**, Figure S12: ^{13}C -NMR spectrum of **6m**, Figure S13: ^1H -NMR spectrum of **6n**, Figure S14: ^1H -NMR spectrum of **6q**, Figure S15: ^{13}C -NMR spectrum of **6q**, Figure S16: ^1H -NMR spectrum of **6r**, Figure S17: ^{13}C -NMR spectrum of **6r**, Figure S18: ^1H -NMR spectrum of **6t**, Figure S19: ^{13}C -NMR spectrum of **6t**, Figure S20: ^1H -NMR spectrum of **6u**, Figure S21: ^{13}C -NMR spectrum of **6u**, Figure S22: ^1H -NMR spectrum of **6v**, Figure S23: ^{13}C -NMR spectrum of **6v**, Figure S24: ^1H -NMR spectrum **6w**, Figure S25: ^{13}C -NMR spectrum of **6w**, Figure S26: ^1H -NMR spectrum **6x**, Figure S27: ^{13}C -NMR spectrum of **6x**.

Author Contributions: Conceptualization, S.A.P. and E.N.Z.; methodology, A.R., S.M.N., M.P. and E.S.; software, S.M.N.; validation, S.A.P. and E.N.Z.; writing—original draft preparation, S.M.N.; writing—review and editing, S.A.P. and E.N.Z.; supervision, S.A.P. and E.N.Z. All authors have read and agreed to the published version of the manuscript.

Funding: This research received no external funding.

Data Availability Statement: Data are available upon request.

Conflicts of Interest: The authors declare no conflict of interest.

References

1. Heidarzadeh, F.; Rahimi, E. Synthesis of 3-substituted Indoles through Yonemitsu Reaction with Copper Benzene-1,3,5-tricarboxylate acid Catalyst. *Mater. Chem. Horizons* **2022**, *1*, 169–176. [[CrossRef](#)]
2. Asadi Nasr, M.; Deinvizadeh, M.; Kiasat, A.R. Fe₃O₄@SiO₂/DABCO(OH) Core-Shell Hybrid Nanocomposite: Efficient Nanomagnetic and Basic Reusable Catalyst in the One-pot Synthesis of Trithiocarbonate Derivatives. *Mater. Chem. Horizons*. **2023**, *in press*. [[CrossRef](#)]
3. Reddy, K.R.; Rajgopal, K.; Kantam, M.L. Copper-alginates: A biopolymer supported Cu(II) catalyst for 1,3-dipolar cycloaddition of alkynes with azides and oxidative coupling of 2-naphthols and phenols in water. *Catal. Letters* **2007**, *114*, 36–40. [[CrossRef](#)]
4. Pourjavadi, A.; Motamedi, A.; Hosseini, S.H.; Nazari, M. Magnetic starch nanocomposite as a green heterogeneous support for immobilization of large amounts of copper ions: Heterogeneous catalyst for click synthesis of 1,2,3-triazoles. *RSC Adv.* **2016**, *6*, 19128–19135. [[CrossRef](#)]
5. Zareh, E.N.; Moghadam, P.N.; Azariyan, E.; Sharifian, I. Conductive and biodegradable polyaniline/starch blends and their composites with polystyrene. *Iran. Polym. J.* **2011**, *20*, 319–328.
6. Sharma, B.; Malik, P.; Jain, P. Biopolymer reinforced nanocomposites: A comprehensive review. *Mater. Today Commun.* **2018**, *16*, 353–363. [[CrossRef](#)]
7. Alizadeh, E.; Baseri, H. Photocatalytic degradation of Sumatriptan Succinate by ZnO, Fe doped ZnO and TiO₂-ZnO nanocatalysts. *Mater. Chem. Horizons* **2022**, *1*, 7–21. [[CrossRef](#)]
8. Heidari, G.; Hassanpour, M.; Nejaddehbash, F.; Sarfjoo, M.R.; Yousefiasl, S.; Sharifi, E.; Bigham, A.; Agarwal, T.; Borzacchiello, A.; Lagreca, E.; et al. Biosynthesized Nanomaterials with Antioxidant and Antimicrobial Properties. *Mater. Chem. Horizons* **2022**, *1*, 35–48. [[CrossRef](#)]
9. Ghorbanipour, F.; Nezhad, S.M.; Pourmousavi, S.A.; Zare, E.N.; Heidari, G. Superparamagnetic polymer nanocomposite as a catalyst for the synthesis of pyrano[3,2-c]chromene, pyrano[2,3-c]pyrazole, and benzylpyrazolyl coumarin. *Inorg. Chem. Commun.* **2023**, *147*, 110271. [[CrossRef](#)]
10. Nakagawa, H.; Ohyama, R.; Kimata, A.; Suzuki, T.; Miyata, N. Hydroxyl radical scavenging by edaravone derivatives: Efficient scavenging by 3-methyl-1-(pyridin-2-yl)-5-pyrazolone with an intramolecular base. *Bioorg. Med. Chem. Lett.* **2006**, *16*, 5939–5942. [[CrossRef](#)]
11. Alam, M.A. Antibacterial pyrazoles: Tackling resistant bacteria. *Future Med. Chem.* **2022**, *14*, 343–362. [[CrossRef](#)] [[PubMed](#)]
12. Vijesh, A.M.; Isloor, A.M.; Isloor, S.; Shivananda, K.N.; Shyma, P.C.; Arulmoli, T. Synthesis of some new pyrazolone derivatives as potent antimicrobial agents. *Der Pharma Chem.* **2011**, *3*, 454–463.
13. Ramajayam, R.; Tan, K.P.; Liu, H.G.; Liang, P.H. Synthesis and evaluation of pyrazolone compounds as SARS-coronavirus 3C-like protease inhibitors. *Bioorg. Med. Chem.* **2010**, *18*, 7849–7854. [[CrossRef](#)]
14. Marković, V.; Erić, S.; Stanojković, T.; Gligorijević, N.; Aranelović, S.; Todorović, N.; Trifunović, S.; Manojlović, N.; Jelić, R.; Joksović, M.D. Antiproliferative activity and QSAR studies of a series of new 4-aminomethylidene derivatives of some pyrazol-5-ones. *Bioorg. Med. Chem. Lett.* **2011**, *21*, 4416–4421. [[CrossRef](#)] [[PubMed](#)]
15. Gunasekaran, P.; Perumal, S.; Yogeewari, P.; Sriram, D. A facile four-component sequential protocol in the expedient synthesis of novel 2-aryl-5-methyl-2,3-dihydro-1H-3-pyrazolones in water and their antitubercular evaluation. *Eur. J. Med. Chem.* **2011**, *46*, 4530–4536. [[CrossRef](#)]
16. Ragab, F.A.F.; Abdel-Gawad, N.M.; Georgey, H.H.; Said, M.F. Pyrazolone derivatives: Synthesis, anti-inflammatory, analgesic quantitative structure-activity relationship and in vitro studies. *Chem. Pharm. Bull.* **2013**, *61*, 834–845. [[CrossRef](#)]
17. Rao, D.J.; Nagaraju, K.; Maddila, S. Microwave irradiated mild, rapid, one-pot and multi-component synthesis of isoxazole-5(4H)-ones. *Chem. Data Collect.* **2021**, *32*, 100669. [[CrossRef](#)]
18. Sivakumar, K.K.; Rajasekaran, A.; Senthilkumar, P.; Wattanwar, P.P. Conventional and microwave assisted synthesis of pyrazolone Mannich bases possessing anti-inflammatory, analgesic, ulcerogenic effect and antimicrobial properties. *Bioorg. Med. Chem. Lett.* **2014**, *24*, 2940–2944. [[CrossRef](#)]
19. Sarfjoo, M.R.; Shad, A.; Hassanpour, M.; Varma, R. An Overview on New Anticancer Drugs Approved by Food and Drug Administration: Impending Economic and Environmental Challenges. *Mater. Chem. Horizons* **2022**, *1*, 189–198. [[CrossRef](#)]
20. Ma, R.; Zhu, J.; Liu, J.; Chen, L.; Shen, X.; Jiang, H.; Li, J. Microwave-assisted one-pot synthesis of pyrazolone derivatives under solvent-free conditions. *Molecules* **2010**, *15*, 3593–3601. [[CrossRef](#)]

21. Malle, A.; Yehualawork, A. This is an electronic reprint of the original article. This reprint may differ from the original in pagination and typographic detail. *Int. J. Spec. Educ.* **2015**, *30*, 70–84.
22. Mousa, S.A.S.; Ishak, E.A.; Bakheet, M.E.M.; Abu-shanab, F.A. New Route for the Synthesis of Pyrazolone Derivatives. *Elixir Org. Chem.* **2015**, *89*, 36854–36859.
23. Yang, Z.; Wang, Z.; Bai, S.; Liu, X.; Lin, L.; Feng, X. Asymmetric α -amination of 4-substituted pyrazolones catalyzed by a chiral Gd(OTf)₃/N,N'-dioxide complex: Highly enantioselective synthesis of 4-amino-5-pyrazolone derivatives. *Org. Lett.* **2011**, *13*, 596–599. [[CrossRef](#)]
24. Isaad, J.; El Achari, A. Synthesis and spectroscopic characterization of azoic dyes based on pyrazolone derivatives catalyzed by an acidic ionic liquid supported on silica-coated magnetite nanoparticle. *J. Mol. Struct.* **2018**, *1154*, 557–564. [[CrossRef](#)]
25. Ekbote, S.S.; Gadge, S.T.; Bhanage, B.M. Synthesis of Pyrazole by Using Polyvinylsulfonic Acid (PVSA) as a Novel Bronsted Acid Catalyst. *Curr. Catal.* **2016**, *5*, 4–10. [[CrossRef](#)]
26. Mojtahedi, M.M.; Javadvpour, M.; Abaee, M.S. Convenient ultrasound mediated synthesis of substituted pyrazolones under solvent-free conditions. *Ultrason. Sonochem.* **2008**, *15*, 828–832. [[CrossRef](#)]
27. Nouri, A.; Jelkmann, M.; Khoee, S.; Bernkop-Schnürch, A. Diaminated Starch: A Competitor of Chitosan with Highly Mucoadhesive Properties due to Increased Local Cationic Charge Density. *Biomacromolecules* **2020**, *21*, 999–1008. [[CrossRef](#)] [[PubMed](#)]
28. Xia, M.; Lu, Y. Solid-state synthesis of 4-[(indol-3-yl)-arylmethyl]-1-phenyl-3-methyl-5-pyrazolones by catalysis of molecular iodine. *Synth. Commun.* **2006**, *36*, 2389–2399. [[CrossRef](#)]
29. Li, X.L.; Wang, Y.M.; Tian, B.; Matsuura, T.; Meng, J. Ben The Solid-State Michael Addition of 3-Methyl-1-phenyl-5-pyrazolone. *J. Heterocycl. Chem.* **1998**, *35*, 129–134. [[CrossRef](#)]
30. Nezhad, S.M.; Pourmousavi, S.A.; Zare, E.N.; Heidari, G.; Makvandi, P. Magnetic sulfonated melamine-Formaldehyde Resin as an efficient catalyst for the synthesis of antioxidant and antimicrobial pyrazolone derivatives. *Catalysts* **2022**, *12*, 626. [[CrossRef](#)]
31. Yusuf, H.; Satria, D.; Suryawati, S.; Fahriani, M. Combination therapy of eurycomanone and doxorubicin as anticancer on T47D and MCF-7 Cell Lines. *Syst. Rev. Pharm.* **2020**, *11*, 335–341.
32. Fang, X.J.; Jiang, H.; Zhu, Y.Q.; Zhang, L.Y.; Fan, Q.H.; Tian, Y. Doxorubicin induces drug resistance and expression of the novel CD44st via NF- κ B in human breast cancer MCF-7 cells. *Oncol. Rep.* **2014**, *31*, 2735–2742. [[CrossRef](#)] [[PubMed](#)]
33. Lovitt, C.J.; Shelper, T.B.; Avery, V.M. Doxorubicin resistance in breast cancer cells is mediated by extracellular matrix proteins. *BMC Cancer* **2018**, *18*, 41. [[CrossRef](#)] [[PubMed](#)]
34. Rouibah, H.; Kebsa, W.; Lahouel, M.; Zihlif, M.; Ahram, M.; Aburmaileh, B.; Mansour Al Shhab, M.A.; Al-Ameer, H.J.; Mustafa, E. Algerian propolis: Between protection of normal cells and potentialisation of the anticancer effects of doxorubicin against breast cancer cells via P-glycoprotein inhibition and cell cycle arrest in the S phase. *J. Physiol. Pharm.* **2021**, *72*, 10–26402.

Disclaimer/Publisher's Note: The statements, opinions and data contained in all publications are solely those of the individual author(s) and contributor(s) and not of MDPI and/or the editor(s). MDPI and/or the editor(s) disclaim responsibility for any injury to people or property resulting from any ideas, methods, instructions or products referred to in the content.